Heating dynamics and extreme ultraviolet radiation emission of laser-produced Sn plasmas

S. Yuspeh,[a] K. L. Sequoia, Y. Tao, M. S. Tillack, R. A. Burdt, and F. Najmabadi
Department of Electrical and Computer Engineering, Center for Energy Research, University of California, San Diego, 9500 Gilman Drive, La Jolla, California 92093-0417, USA

(Received 17 February 2010; accepted 9 June 2010; published online 30 June 2010)

The impact of 1.064 μm laser absorption depth on the heating and in-band (2% bandwidth) 13.5 nm extreme ultraviolet emissions in Sn plasmas is investigated experimentally and numerically. In-band emission lasting longer than the laser pulse and separation between the laser absorption and in-band emission region are observed. Maximum efficiency is achieved by additional heating of the core of the plasma to allow the optimal temperature to expand to a lower and more optically thin density. This leads to higher temperature plasma that emits less in-band light as compared to CO_2 produced plasma sources for the same application. © *2010 American Institute of Physics*. [doi:10.1063/1.3458696]

In recent years a great deal of research effort has focused on Sn laser-produced plasmas (LPPs) for a 13.5 nm extreme ultraviolet (EUV) light source for next generation lithography for semiconductor microchips with nodes 32 nm and below. The high cost of ownership of high power lasers makes the conversion efficiency (CE), laser to 13.5 nm (2% bandwidth) EUV light in a solid angle of 2π steradian, a key figure of merit for an EUV source. The 13.5 nm wavelength requirement comes from the reflective optics available, i.e., multilayer Mo/Si mirrors.[1] For Sn based plasmas the majority of the in-band EUV is generated by an unresolved transition array produced by Sn^{5+} to Sn^{14+}.[2]

The two regions of interest in a Sn LPP are an inner core known as the EUV dominant emitting region (DER) where a majority of the in-band light is generated and a surrounding colder, lower density plasma that absorbs the in-band EUV light.[3] However, for neodymium doped yttrium aluminum garnet (Nd:YAG) 1.064 μm laser operating at intensities to maximize CE, most of the DER is optically thick to EUV. A majority of the EUV never escapes from the DER and only the in-band EUV generated near the outer surface of the DER escapes.[4] By moving to a longer wavelength, e.g., 10.6 μm, the laser absorption and DER occur at lower densities which are optically thin to EUV and thus leads to a large increase in CE.[5,6] In this paper, we show the impact of the laser absorption depth for an Nd:YAG Sn LPP x-ray source on the electron temperatures and EUV emissions using a combination of experimental results coupled with numerical simulations. Brief comparisons between the results and previous CO_2 experiments are also discussed.

The targets were fabricated by sputtering 2–3 μm of 5N pure Sn onto a 280 μm diameter glass bead. The plasma was generated by focusing a 7 ns full width half maximum (FHWM) Nd:YAG laser to a $1/e^2$ diameter spot of 150 μm with an energy of 250 mJ. A second Nd:YAG laser with a pulse length of 130 ps FWHM operating at 532 nm was used as a probe beam orthogonal to the main heating beam in a Nomarski interferometer. More details of the general experimental arrangement can be found elsewhere.[5]

A back-illuminated x-ray CCD camera was employed in a time-integrated in-band EUV imaging system. A multilayer concave Mo/Si mirror is placed perpendicular to the pump beam and focuses the EUV light with FWHM bandwidth of 0.5 nm centered at 13.5 nm to the camera. The entire path is shielded and a Zr filter blocks the visible spectrum.[7]

Time-resolved EUV emissions at 45° from the pump beam were recorded by using a single Mo/Si mirror along with a filtered pinhole x-ray diode (XRD) with a fall time of 150 ps. The mirror reflects the EUV and visible light from the plasma to the diode and the filter on the XRD removes the visible light. The heating laser pulse was simultaneously recorded using a fast photodiode with a 350 ps fall time.

The electron temperature cannot be experimentally measured for small-scale length plasmas such as the one discussed in this work due to the steep gradients in both temperature and density. Therefore, numerical simulations were performed to obtain temperature profile maps.

The H2D code solves the two-fluid radiation hydrodynamics equations in a two-dimensional Lagrangian coordinate system.[8] H2D was operated using an average-atom local thermal equilibrium, tabular equation of states derived from the Los Alamos National Laboratory T4 SESAME tables, and Rosseland mean opacities for the atomic physics, radiation transport and flux-limited gray radiation diffusion, respectively. The parameters of the H2D simulation matched those of the experiment.

Figure 1(a) shows a comparison between the simulated and recorded electron density at the peak of the laser pulse. Only electron densities in the range of a few 10^{19}–10^{17} cm^{-3} are shown due to diagnostic limitations. The algorithm used to process interferograms into density profile maps is presented elsewhere.[9] If the simulation accurately models the plasma conditions, the two profiles should be mirror images of one another. The numerical simulation agrees with the experimental measurements to within a factor of two in the domain of interest (100–500 μm from the target surface).

For a LPP, the plasma density scale length is related to the plasma temperature by $l_s = \sqrt{ZT_e/M_i}\tau_{\text{Laser}}$, where l_s is the plasma scale length, Z is the average charge state, T_e is the plasma temperature, M_i is the ion mass, and τ_{Laser} is the laser pulse duration.[10] Therefore, the plasma density profile is di-

[a]Electronic mail: syuspeh@ucsd.edu.

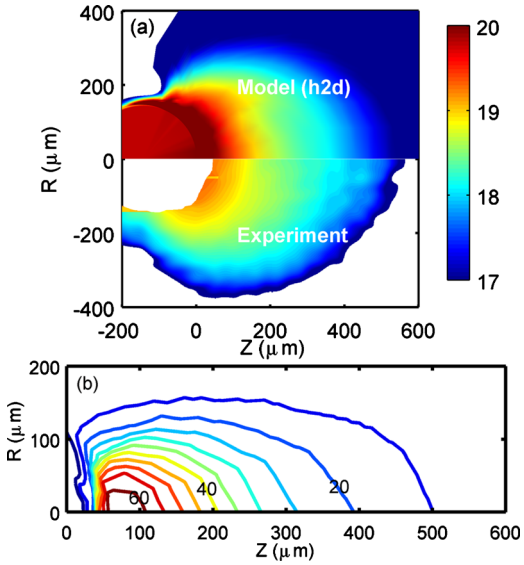

FIG. 1. (Color online) (a) Log_{10} of the electron density at the peak of the laser pulse for a H2D simulation (top) and a typical experiment (bottom). (b) Electron temperature contour lines at the peak of the laser pulse for 60–10 eV in 5 eV increments.

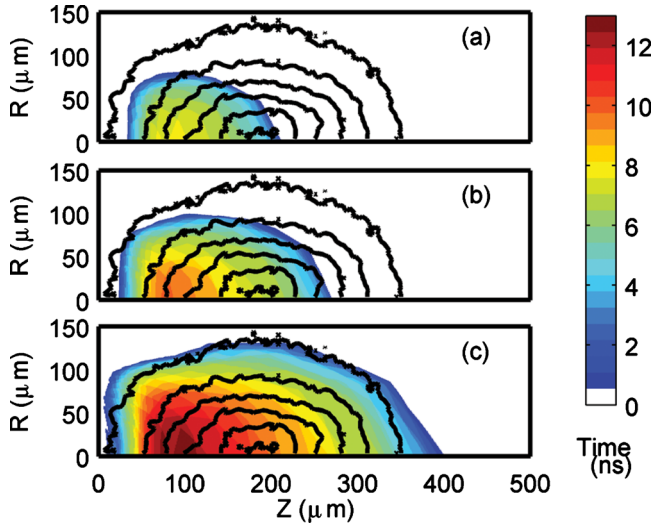

FIG. 2. (Color online) Time-integrated profile maps of the simulated (a) 20 eV, (b) 30 eV, and (c) 40 eV electron temperature surfaces. Plotted on top of those images are 0.9–0.15 of normal in 0.15 increments of a typical experimentally recorded in-band EUV image.

rectly related to the plasma temperature. Fitting of the exponential decay function $\exp(-x/l_s)$ of the plasma density along the laser axis give scale lengths at the peak of the laser pulse of 110 and 125 μm for the H2D and experimental plasmas, respectively. The simulated peak electron temperature was 20% lower than the temperature calculated from the experiment at the peak of the laser pulse. The shorter scale length from the simulation is most likely due to the absence of bound-bound transitions in H2D, where most of the EUV is generated.[11] Without bound–bound transitions, the amount of EUV light being generated in the model will be reduced. However, the amount of EUV light being generated is relatively small compared to the rest of the radiation of the plasma. The lower amount of EUV will only affect regions of high EUV absorption, which is the optical thick region close to the target surface. This leads to a lower density near the target surface [seen in Fig. 1(a)] thus resulting in a smaller scale length and a slightly lower plasma temperature.

At the optimal laser intensity for the highest CE, which is discussed here, the core of the plasma is heated to electron temperatures higher than 60 eV, which is more than double the optimal temperature of 30 eV to produce in-band EUV emission. Additionally, it has been shown that the spectral efficiency decreases rapidly with temperatures above 40 eV for densities above $10^{17}\mathrm{n_e}$ cm^{-3}.[11] To understand this phenomenon, further investigation of the location where the detected in-band EUV light is being generated is required.

Figure 2 shows time-integration of the simulated electron temperature surface, which shows in two-dimensional space, the lifetime of the indicated electron temperature of (a) 20 eV, (b) 30 eV, and (c) 40 eV. Contours of a typical experimental time-integrated in-band EUV image are plotted over Figs. 2(a)–2(c). The figures were generated by rotating a single electron temperature contour line about the Z-axis and integrating the contour surface over the time duration of the plasma. Ignoring opacity effects for the time being, the time-integrated electron temperature surfaces show the possible size and shape of the DER assuming only the 20, 30, or 40 eV plasma contributes to detected in-band emissions. Spatially, only the 20 eV plasma surface closely matches the recorded DER. This shows that the 20 eV surface is responsible for the detected in-band emission. Further support of the 20 eV surface producing the detected in-band EUV will be discussed later.

Figure 3(a) shows simulations of electron density, electron temperature, and laser absorption at the peak of the laser pulse as well as the experimentally recorded in-band EUV emission along the laser axis. The majority of the laser absorption occurs in a region 40–100 μm from the target surface corresponding to electron densities from 9.4×10^{20}–$3\times10^{19}\mathrm{n_e}$ cm^{-3}. The hot inner core of the plasma (above 50 eV) is slightly shifted from the laser absorption region, reaching a peak temperature of 63 eV at a distance of 55 μm

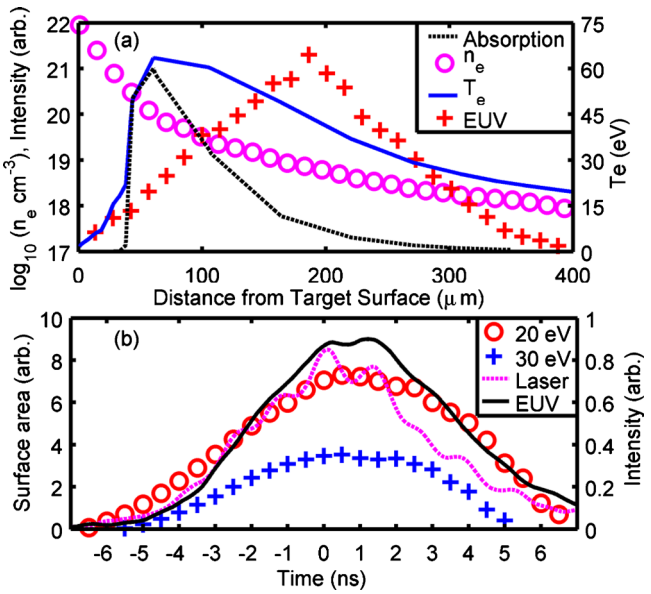

FIG. 3. (Color online) (a) H2D simulated electron density (purple circles), electron temperature (blue line), and laser absorption (black dashes) at the peak of the laser pulse and the experimental time integrated in-band EUV emission (red plus signs) all along the laser axis. (b) H2D simulated cross sectional area of the 20 eV (red circles) and 30 eV (blue plus signs) plasma temperatures along with the experimental laser pulse (purple dashes) and EUV emissions at 45° (black line).

from the target surface. Looking at this inner core from the side (same as the in-band EUV imaging system), the 20 eV plasma surface is present for the longest time period at the location of peak laser absorption, which is approximately the peak temperature location. Thus, this area emits in-band EUV for the longest time period. However, the highest in-band emission does not come from this region but rather is shifted 140 μm away from the peak of the laser absorption.

This separation between the peak laser absorption and the in-band EUV emission location is due to the laser absorption occurring at an optically thick density to in-band EUV. High electron densities (above $5\times10^{19}n_e$ cm^{-3}) near the target surface reduce the in-band EUV CE. Despite the plasma being at the proper temperature for the longest period of time, the density is too high for the EUV emissions to escape from the plasma. The laser intensity required to produce the highest CE "overheats" (beyond optimal temperatures for in-band EUV generation) the core of the plasma until the lower density plasma is heated to 20–30 eV where the in-band EUV can escape from the plasma. The overheating of the plasma is necessary for the highest possible CE with a Nd:YAG laser because the laser wavelength is too short.

The surface area of electron temperature contour surfaces are plotted in Fig. 3(b) along with the recorded in-band EUV emissions and laser pulse profiles. The rising edge of the EUV emissions and the laser pulse are nearly identical. The peak of the EUV emission occurs about 0.5 ns after the peak of the pulse. Again, the simulation of the 20 eV surface best matches the experimental result, lasting 1 ns longer than the laser pulse. The dominant in-band EUV emitting surface is confirmed both spatially and temporally to be generated by approximately the 20 eV plasma surface.

The in-band EUV emission lasting 1 ns longer than the laser pulse is caused by the overheating of the plasma. After the peak of the laser pulse, the plasma begins to cool and the EUV emission follows the plasma temperature. The dense overheated core of the plasma contains additional energy that is transmitted to the lower density plasma allowing for continued in-band emission. In-band emission lasting longer than the pulse length at the optimal laser intensity for that wavelength signifies that the laser absorption is occurring at an optically thick density. Therefore a longer wavelength laser would produce higher CE assuming the amount of laser absorption is identical. The temporal in-band emission profile can be used as experimental verification that the laser is being absorbed at an optically thick density to in-band light.

Using a 2.2 ns pulse at the optimum power density for CE (5×10^{10} W/cm^2), modeling by White *et al.*[12,13] has shown similar overheating of the core and predicts the EUV emission lagging the laser pulse. However, Shimada *et al.*[14] only observed EUV emission lagging the laser at much higher than optimal laser intensity. A possible explanation for not observing the lag at the optimal intensity could be spectral bandwidth of the detector (12–17 nm) is too large, since the temporal emission profile is wavelength dependent. In the experiment of Shimada *et al.*, the hot core of the plasma (40–70 eV) emits shorter wavelength light that the photodiode detects which would be considered out-of-band in our system. The lower optimum intensity in other experiments is due to different conditions (pulse length, target geometry, and spot size).

The necessity to overheat the plasma to overcome the absorption depth is a main reason that Nd:YAG laser produce lower CE than CO_2 lasers. Even with lower laser absorption efficiency into the plasma, CO_2 lasers produce CEs of 3%–4% at intensity of 10^9-10^{10} W/cm^2 while Nd:YAG lasers are around 2% at a few 10^{11} W/cm^2.[5] The effects of overheating are not observed in plasmas generated by 10.6 μm CO_2 lasers, where absorption takes place at optically thin densities. Tao *et al.*[15] shows that the peak of the DER is very close to the critical density. Even for long CO_2 laser pulses, the DER propagation follows the expansion of the critical density surface. Also the in-band EUV emission follows the CO_2 laser pulse.[6] The CO_2 Sn LPPs created at intensities to maximize CE do not overheat the core. Therefore, the CO_2 generated plasma peak temperature is lower than that produced by the shorter wavelength Nd:YAG laser.

In summary, the physics behind the relationship between the Nd:YAG Sn LPP laser absorption, electron temperature and in-band EUV emissions are discussed. At optimal laser intensity, the EUV emissions last longer than the laser pulse and the laser absorption and EUV emissions occur at different locations. The plasma is overheated to force the emitting surface to expand outward to a lower density allowing the generated in-band emission to escape the plasma. This overheating is not necessary when CO_2 lasers are used for heating the plasma.

S. Yuspeh and K. L. Sequoia contributed equally to this work. The authors would like to acknowledge both General Atomics and Cascade Applied Sciences, Inc., for the use of and support with H2D. This work was supported by KLA-Tencor, Cymer, Inc., and by the University of California (UC) under the UC Industry-University Cooperative Research Program.

[1] S. Bajt, J. Alameda, T. Barbee, Jr., W. Clift, J. Folta, B. Kaufmann, and E. Spiller, Opt. Eng. (Bellingham) **41**, 1797 (2002).
[2] G. O'Sullivan and R. Faulkner, Opt. Eng. (Bellingham) **33**, 3978 (1994).
[3] K. L. Sequoia, Y. Tao, S. Yuspeh, R. Burdt, and M. S. Tillack, Appl. Phys. Lett. **92**, 221505 (2008).
[4] Y. Tao, S. S. Harilal, M. S. Tillack, K. L. Sequoia, B. O'Shay, and F. Najmabadi, Opt. Lett. **31**, 2492 (2006).
[5] J. White, P. Dunne, P. Hayden, F. O'Reilly, and G. O'Sullivan, Appl. Phys. Lett. **90**, 181502 (2007).
[6] Y. Tao, M. S. Tillack, K. L. Sequoia, R. A. Burdt, S. Yuspeh, and F. Najmabadi, Appl. Phys. Lett. **92**, 251501 (2008).
[7] S. Yuspeh, K. L. Sequoia, Y. Tao, M. S. Tillack, R. Burdt, and F. Najmabadi, Appl. Phys. Lett. **93**, 221503 (2008).
[8] J. Larson, in H2D is a commercial product of Cascade Applied Sciences Incorporated, 6325 Trevarton Drive,Longmont, CO 80503. Electronic mail: larsen@casinc.com.
[9] L. B. Da Silva, T. W. Barbee, R. Cauble, P. Celliers, D. Ciarlo, S. Libby, R. A. London, D. Matthews, S. Mrowka, J. C. Moreno, D. Ress, J. E. Trebes, A. S. Wan, and F. Weber, Phys. Rev. Lett. **74**, 3991 (1995).
[10] W. Kruer, *The Physics of Laser Plasma Interactions* (Westview, Boulder, 2003).
[11] A. Sasaki, A. Sunahara, K. Nishihawra, T. Nishikawa, F. Koike, and H. Tanuma, J. Phys.: Conf. Ser. **112**, 042062 (2008).
[12] J. White, G. O'Sullivan, S. Zakharov, P. Choi, V. Zakharov, H. Nishimura, S. Fujioka, and K. Nishihara, Appl. Phys. Lett. **92**, 151501 (2008).
[13] J. White, presented at the Sematech EUV Source Workshop, Baltimore (2009); www.sematech.org.
[14] Y. Shimada, H. Nishimura, M. Nakai, K. Hashimoto, M. Yamaura, Y. Tao, K. Shigemori, T. Okuno, K. Nishihara, and T. Kawamura, Appl. Phys. Lett. **86**, 051501 (2005).
[15] Y. Tao, M. Tillack, S. Yuseph, R. Burdt, and F. Najmabadi, Appl. Phys. B: Lasers Opt. **99**, 397 (2010).